



## Research article

## Fine-tuning the dye adsorption capacity of UiO-66 by a mixed-ligand approach

Chompoonoot Nanthamathee<sup>a,b</sup>, Chantamalinee Chantarangkul<sup>a</sup>, Chanida Jakkrawhad<sup>a</sup>, Apirak Payaka<sup>a</sup>, Pongsathorn Dechatiwongse<sup>c,\*</sup><sup>a</sup> Department of Chemistry, School of Science, Walailak University, Nakhon Si Thammarat, 80160, Thailand<sup>b</sup> Center of Excellence on Wood and Biomaterials, Walailak University, Nakhon Si Thammarat, 80160, Thailand<sup>c</sup> Department of Chemical Engineering, School of Engineering and Technology, Walailak University, Nakhon Si Thammarat, 80160, Thailand

## ARTICLE INFO

## Keywords:

Mixed-ligand approach  
Metal-organic frameworks  
Indigo carmine  
UiO-66  
Adsorption capacity

## ABSTRACT

The mixed ligand synthetic approach offers an alternative to engineering a specific character in metal-organic framework (MOFs) materials. Herein, we synthesized and characterized a well-known prototype zirconium-based-MOF, so-called UiO-66, and its mixed ligand derivatives UiO-66-xATA, where x is mole fraction (0.5, 0.75, and 1.0) and ATA is 2-animoterephthalate. The study investigates whether the dye adsorption capacity can be tuned/enhanced by the ATA ligand substitution into the framework. We found that, at room temperature, UiO-66-0.75ATA shows the highest adsorption capacity toward various dye solutions, including methylene blue (MB), indigo carmine (IC), and congo red (CR). The optimum adsorption conditions in all four materials were in a common trend where their adsorption capacities can be increased with decreasing pH and adsorbent dose, increasing IC concentration, contact time, and temperature. Pseudo-second order kinetics model fits best with their adsorption data, where UiO-66-ATA has the fastest adsorption rate. Langmuir and Freundlich isotherms were found best to describe adsorption behavior in ATA-containing UiO-66 and UiO-66, respectively, where adsorption processes were found to be physisorption. Confirming by thermodynamic studies, the adsorption in all four materials occurred spontaneously, driven by entropy. Computational studies showed ligand to metal charge transfer where the distribution of electron densities was varied with the amount of functionalized ligand. Adsorption mechanism is proposed as a synergistic interplay between electrostatic interaction and hydrogen bonding. The findings in this work broaden the potential strategy to fine-tune the dye adsorption capacity in MOF materials.

## 1. Introduction

Serving for human's daily life necessities, textile is one of the world's most important industries with the worth of its global industry estimated at US\$1 trillion worldwide (Thiry, 2011). Due to the continuously increasing global population, there has been a substantial expansion of such a sector worldwide. During textile processing, various dyes are discharged into water effluent on a large scale, estimated to account for more than 35% of chemicals released in the environment (Desore and Narula, 2018). As a result, there have been tremendous and wide concerns on water pollution and its impact on the environment, as compounds within dyes, e.g. aromatics, metals and chlorides, are potentially toxic to living organisms, including aquatic life and humans. Therefore, it is very important that dye-contaminated water effluents must be properly treated before being discharged into the water environment. So far,

various methods have been developed to treat dye wastewater, e.g. membrane filtration, chemical treatment, incineration, adsorption, and biological oxidation. Among these methods, adsorption on porous materials is a promising approach because of its simplicity, low cost, and ease of operation.

Metal-organic frameworks (MOFs) composed of secondary building units (SBUs) with organic ligands through coordinate covalent bonds have been widely investigated because of their excellent physicochemical property as adsorbents. Up to now, research studies have been conducted on several MOFs, e.g., MIL-53 (Li et al., 2015), MIL-100 (Huo and Yan, 2012), MIL-101 (Chen et al., 2012), HKUST-1 (Xu et al., 2015), CuBTC (Nanthamathee, 2019), and UiO-66 (Mohammadi et al., 2017). Although these MOFs show high adsorption capacity, their stability under an aqueous solution can obstruct the practical application. Among all previously investigated MOFs, UiO-66 is the most promising

\* Corresponding author.

E-mail address: [pongsathorn.dechatiwongse@gmail.com](mailto:pongsathorn.dechatiwongse@gmail.com) (P. Dechatiwongse).<https://doi.org/10.1016/j.heliyon.2022.e08961>

Received 10 October 2021; Received in revised form 12 December 2021; Accepted 10 February 2022

2405-8440/© 2022 The Author(s). Published by Elsevier Ltd. This is an open access article under the CC BY-NC-ND license (<http://creativecommons.org/licenses/by-nc-nd/4.0/>).

candidate for removing dye from an aqueous solution, as its framework remains intact after soaking in the solution for up to a year (Molavi et al., 2018).

UiO-66 ( $Zr_6O_4(OH)_4(BDC)_{12}$ ) is a zirconium-based MOF made up of [ $Zr_6O_4(OH)_4$ ] SBUs linked with 1,4-benzenedicarboxylic acid. Because of its structure, UiO-66 exhibits a large surface area, excellent pore volume, and high stability toward external stimuli such as heat, chemicals, and pressure. As a result, it can endure strong basic and acidic solutions and organic solvents, having great potential in wastewater treatment. So far, the adsorption performance of UiO-66 has been successfully investigated on several systems, including dyes (Ahmadijokani et al., 2020; Han et al., 2017; Molavi et al., 2018; Qiu et al., 2017; Yang, 2017; Yang et al., 2018) pharmaceuticals and personal care products (PPCPs) (Hasan et al., 2016), and toxic pollutants (Rego et al., 2021). The adsorption capacity is governed by intramolecular forces generated between the UiO-66 framework's surface and the dye molecules. As such, several attempts have been made to understand how these intramolecular forces affect the adsorption process and thus find possible ways to improve the adsorption performances of UiO-66. Previous attempts include (1) use of novel synthesis process (2) introduction of mixed metal into SBUs (3) introduction of mixed ligand into framework (4) modification of surface charge via treatment with acid or base and (5) modification of surface charge via ligand functionalization.

The concept of mixed-component metal-organic framework (MC-MOFs) is a worth investigating option for enhancing UiO-66 adsorption performance. As MOFs have tunable porosities and thus, they can be tailor-made to have heterometallic SBUs or different ligands connected to SBUs. By modification of metals or ligands, synthesized MC-MOFs could offer multifunctionality, and their intrinsic properties, which could be fine-tuned to be suitable for a specific application. MC-MOFs can be classified into two major groups, i.e. (1) mixed-metal (MM-MOFs) and (2) mixed-ligand MOFs (ML-MOFs). While the former is defined as those MOFs having more than one metal somewhere in their structure, the latter is referred to as those having more than one type of ligand in the framework (Masoomi et al., 2019). Due to the synergy that could derive from the presence of mixed components, several studies reported superior performance of MC-MOFs in dye adsorption compared to mono-component MOFs.

In the case of UiO-66, superior performance for dye adsorption by its MM-MOFs has been reported when the insertion of Ce(III) or Ti(IV) ions were doped into the material framework (Han et al., 2017; Yang et al., 2018). Moreover, the incorporation of Ag nanoparticles into the UiO-66 framework boosted the dye adsorption capacity by 400% (Salama et al., 2021). In contrast, there is still no study made to investigate its mixed-ligand performance on the dye removal from an aqueous solution, which thus became the aim of this study.

In this study, mixed ligand UiO-66 (ML-UiO-66) was synthesized by variation of ligands between terephthalic acid (BDC) and 2-aminoterephthalic acid (ATA) in the molar ratio of 1:0, 0.5:0.5, 0.25:0.75 and 0:1 and then characterized by several techniques. The dye adsorption performance of all synthesized MOFs was examined using indigo carmine (IC), the organic compound most associated with denim cloth and blue jeans production. Up to our best knowledge, this is the first time investigation on IC removal from an aqueous solution by UiO-66-ATA and its mixed ligand derivatives. The adsorption parameters, adsorption isotherms, adsorption kinetics, and adsorption thermodynamics of all synthesized materials were also studied to investigate the effect of the mixed ligand approach on UiO-66 adsorption capacity. The possible mechanisms of the adsorption process were also suggested and discussed.

## 2. Experimental section

### 2.1. Syntheses of the adsorbents

UiO-66, mixed-ligand UiO-66, and UiO-66-ATA were synthesized using a solvothermal route according to the previously reported

procedure where no modulator was added during the syntheses (Cavka et al., 2008). The chemicals purchased commercially were used directly without any further purification. The detail of the synthesis of each adsorbent are described in the following section.

#### 2.1.1. UiO-66

UiO-66 was synthesized by adding 0.7768 mg of  $ZrCl_4$  in 20.0 mL of DMF. Once the metal salt was completely dissolved, 0.5538 g of BDC was added to the solution. The solution was transferred into a 45 mL Teflon-liner autoclave and heated to 120 °C overnight. The mixture was let cool for a day before the filtration. The fine white powder was recovered and washed with DMF and methanol several times before drying overnight at 70 °C. Before calcination, 1.000 g of as-made materials was stirred overnight in 20 mL of methanol and recovered by filtration. After let dried, methanol-treated material was activated at 573 K for 12 h under ambient conditions.

#### 2.1.2. UiO-66-0.5ATA

Mixed-ligand UiO-66 was synthesized using the same procedure as was in the synthesis of UiO-66. 0.7768 mg of  $ZrCl_4$  was dissolved well in 20.0 mL of DMF before 0.2769 g of BDC and 0.3019 g of ATA were subsequently mixed into the solution and stirred vigorously. The solution was heated in a 45 mL Teflon-liner reactor at 120 °C for 24 h. Pale yellow powder was recovered and rinsed with DMF and methanol. The product was then let dried at 70 °C.

#### 2.1.3. UiO-66-0.75ATA

For UiO-66-0.75ATA, 0.7768 mg of  $ZrCl_4$  was dissolved well in 20.0 mL of DMF before 0.1385 g, and 0.4529 g of BDC and ATA were subsequently mixed into the solution and stirred vigorously. The solution was heated in a 45 mL Teflon-liner reactor at 120 °C for 24 h. Pale yellow powder was recovered and rinsed with DMF and methanol. The product was then let dried at 70 °C.

#### 2.1.4. UiO-66-ATA

UiO-66-ATA is isostructural to UiO-66. Therefore, its synthetic process was conducted using a similar procedure to UiO-66. 0.7768 mg of  $ZrCl_4$  was added in 20.0 mL of DMF and stirred until completely dissolved. 0.6038 g of 2-amino-1, 4-benzenedicarboxylic acid (ATA) was then mixed into the solution and stirred. The homogenous solution was transferred in a 45 mL Teflon-liner reactor and heated to 120 °C overnight. After the mixture was cooled, the pale-yellow powder was filtered and washed several times with DMF and methanol. The product was dried at 70 °C before activation.

### 2.2. Activation of the adsorbents

The as-made adsorbents were treated with methanol prior to the calcination in order to exchange with the unreacted starting materials inside the framework. This process leads to a lower calcination temperature, preventing the framework from decomposition. Basically, 1.0 g of the adsorbent was stirred overnight in 20.0 mL methanol. The adsorbent was then recovered by filtration and dried in the oven at 70 °C. The methanol-treated adsorbents were calcined at different temperatures and duration, depending on their decomposition temperature. The calcination temperatures (K)/time (hr.) for UiO-66, UiO-66-0.5ATA, UiO-66-0.75ATA and UiO-66-ATA were 573/12, 493/9, 473/12 and 493/12 respectively. Interestingly, UiO-66 containing ATA ligand required lower calcination temperature, suggesting that their thermal stability was lower than the pristine UiO-66. After the calcination, the calcined adsorbents were kept in the desiccator until used.

### 2.3. Characterization of the synthesized adsorbents

In this study, several techniques were employed for characterizing all synthesized MOFs. Powder X-ray diffraction patterns (PXRD) were

collected using a powder X-ray diffractometer with Cu K $\alpha$  radiation (X'Pert MPD, Philips, USA). Obtained PXRD patterns were matched with the calculated pattern using Mercury 3.9. The crystal morphology of the adsorbents was investigated using a field-emission scanning electron microscope (Merlin compact, Carl Zeiss, Germany). Thermogravimetric analysis was performed at 50.0–800.0 °C with a heating rate of 10 °C/min. In addition, the porosity of the samples, including surface area, pore size, and pore volume, were investigated using N<sub>2</sub> adsorption/desorption isotherms. The materials were degassed at 423 K under high vacuum for 12 h before performing surface area analysis (ASAP2460, Micromeritics, USA).

#### 2.4. Dye adsorption experiments

The stock solution of indigo carmine (IC) was produced at a concentration of 1 g/L and kept at room temperature. To make IC solution at varied concentrations, successive dilutions of the stock solution with deionized water were utilized. pH, adsorbent dosage, starting dye concentration, and contact duration were optimized. In every experiment, 10.000 mg of the adsorbent was dispersed in 10.000 mL IC solution except that in the adsorbent dose experiment, a variation amount from 10.000 mg, 20.000 mg, ..., 100.000 mg was used instead. The pH of the solution was fixed at 6.50 while, for the pH-dependent study, pH of the IC solution was varied by an addition of 0.1 M HCl or 0.1 M NaOH. The incubator shaker, which operated at a predetermined shaking rate of 200 rpm and a fixed temperature of 303 K, was used to guarantee that the IC solutions and adsorbents were thoroughly mixed. The mixtures were left overnight until reaching equilibrium. IC solution after adsorption was achieved by centrifugation at 3,000 rpm for 5 min. The absorbance at 464 nm was determined using a UV-Vis spectrophotometer, which was then used to compute the concentration of IC solution. The data from the adsorption studies were used to fit several kinetic models, including pseudo-first-order, pseudo-second-order, and Elovich kinetic models, in which the rate-limiting step and diffusion mechanism of IC adsorption by all adsorbents were investigated using the intra-particle diffusion model (IPD) (Ezugwu et al., 2019) and Boyd kinetic (Singh et al., 2015). The change of adsorption capacity with initial concentration at selected temperatures was fitted with Langmuir (1916), Freundlich (1906) Dubunin-Radhsbkevisk (D-R), and Temkin isotherm. Later, adsorption thermodynamics parameters including enthalpy ( $\Delta H$ ), entropy ( $\Delta S$ ), and Gibbs free energy ( $\Delta G$ ) for all four MOFs under 303, 313, and 323 K were calculated.

#### 2.5. Computational details

All possible SBU structures of UiO-66, UiO-66-0.5ATA, UiO-0.75ATA and UiO-66-ATA which are  $[\text{Zr}_6\text{O}_4(\text{OH})_4(\text{OOC}-\text{C}_6\text{H}_4-\text{COO})_{12}]^{12-}$ ,  $[\text{Zr}_6\text{O}_4(\text{OH})_4(\text{OOC}-\text{C}_6\text{H}_4-\text{COO})_6(\text{OOC}-\text{C}_6\text{H}_6\text{N}-\text{COO})_6]^{12-}$ ,  $[\text{Zr}_6\text{O}_4(\text{OH})_4(\text{OOC}-\text{C}_6\text{H}_4-\text{COO})_3(\text{OOC}-\text{C}_6\text{H}_6\text{N}-\text{COO})_9]^{12-}$  and  $[\text{Zr}_6\text{O}_4(\text{OH})_4(\text{OOC}-\text{C}_6\text{H}_6\text{N}-\text{COO})_{12}]^{12-}$  respectively, were created and optimized at PM6 level of theory. The optimized structures (Figure S13) were then subjected to excited-state calculations using TD-DFT calculations at PBE1PBE/LanL2DZ level of accuracy. All calculations were performed by the Gaussian09 program package (Frisch et al., 2016). Additionally, the orbitals of the highest occupied molecular orbital (HOMO) and lowest unoccupied molecular orbitals (LUMO) of all structures (Figure S14) were generated by GaussView 5.0 program (R. Dennington, 2009).

### 3. Results and discussions

#### 3.1. Characterization of UiO-66 and its analogues

PXRD patterns of UiO-66, UiO-66-0.5ATA, UiO-66-0.75ATA, and UiO-66-ATA were constructed and present in Figure 1 (a), while the morphology of all as-made adsorbents were shown in Figure S1. From Figure 1 (a), a good agreement between the PXRD pattern of UiO-66

sample and that of UiO-66 modelled from crystallographic data (cubic, space group: Fm-3m with  $a = 20.7004$  (2) and  $Z = 1$ ) was observed and thus confirmed the successful synthesis of the compound (Cavka et al., 2008). In addition, PXRD patterns of two mixed ligand UiO-66 (i.e., UiO-66-0.5ATA and UiO-66-0.75ATA) and UiO-66-ATA also correspond well with that of the UiO-66 sample as well as the simulated one, suggesting that they all are isostructural to UiO-66. Further confirmation was made by employing FTIR spectroscopy, as shown in Figure 1 (b). The figure presents IR spectra of both IC dye and adsorbents before and after adsorption. The spectra of all four pre-adsorbed MOFs show characteristic peaks, which confirms the formation of the framework. These peaks contain two sites about  $600\text{ cm}^{-1}$  and  $700 - 900\text{ cm}^{-1}$ , which correspond to  $\mu^3$ -OH and Zr-O stretching vibrations, respectively. There are also two significant peaks at  $1400$  and  $1590\text{ cm}^{-1}$ , which indicate asymmetric and symmetric stretching in OCO, respectively, and one weak peak at roughly  $1500\text{ cm}^{-1}$ , which represents vibration of C=C in a benzene ring. The successful synthesis of the two mixed ligand UiO-66 and UiO-66-ATA was also confirmed, as the IR spectra show characteristic peaks at  $1255$  together and  $1370\text{ cm}^{-1}$ , representing C-N stretching in the aromatic carbon and nitrogen, and  $1622\text{ cm}^{-1}$ , representing N-H bending vibration, all of which belong to the chemical characteristic of ATA ligands. After IC adsorption, the spectra of all four materials display characteristic peaks of IC dye, e.g. asymmetric and symmetric S-O stretching vibrations at  $1031$  and  $1105\text{ cm}^{-1}$  and asymmetric stretching vibration in S=O at  $1323$  and  $1369\text{ cm}^{-1}$ . As a result, these confirm the adsorption of IC molecules onto the adsorbent. In addition, confirmation can be made by observing changes in spectral intensity. Noticeably, the transmittance intensity of the O-C-O vibration and the N-H vibration becomes decreased after IC adsorption, thereby suggesting that there are adsorbent-adsorbate interactions.

The thermal stability of all four MOFs was investigated using TGA, and the result is illustrated in Figure 1 (c). The figure shows that all materials have similar TGA patterns, which can be divided into three distinct temperature regions. The first one, from the temperature of  $298 - 373\text{ K}$ , displays sharp and initial drops in weight percentage of samples, corresponding to the loss of water or methanol molecules caused by vaporization. The second range, from  $373$  to  $648\text{ K}$ , shows nearly flat profiles, which imply an absence of guest molecules and thus confirm the successful material activation. Reasonably, the weight loss during this region is attributed to the dehydroxylation of the zirconium oxo-clusters. The third region is marked by another significant weight loss, which indicates the organic ligand departure or the framework decomposition. Notably, MOFs' thermal stability appears to decrease as the loading of ATA linkers in the MOFs increases. Numerically, the decomposition temperature of UiO-66, UiO-66-0.5ATA, UiO-66-0.75ATA, and UiO-66-ATA were determined to be  $700$ ,  $653$ ,  $613$  and  $573\text{ K}$ , respectively. These observations agree with the previous study, which reported the decreasing trend of MOFs thermal stability with the rising ATA ligands (Ferreira et al., 2013).

In addition, results from TGA analysis also enable the estimation of missing organic linker numbers by comparing the weight loss percentage occurring during the last region. As labelled on Figure 1 (c), the actual loss of UiO-66, UiO-66-0.5ATA, UiO-66-0.75ATA and UiO-66-ATA are found to be  $36$ ,  $30$ ,  $40$  and  $30\%$ , respectively, all of which are lower than the theoretical loss that could be observed in the perfect UiO-66 ( $54\%$ ) or UiO-66-ATA ( $57\%$ ). The differences in loss values could be rationalized by the defect of either the missing ligand or cluster. Nevertheless, the latter can be eliminated, as our PXRD, Figure 1 (a), shows no characteristic peak at  $2\theta$  of  $2 - 7^\circ$ . Subsequently, it infers missing ligand defects as a cause of discrepancies, which is consistent with the previous study (Ezugwu et al., 2019). The ligand weight loss found in the UiO-66 sample is also in a good agreement with previous reports, which indicate the missing of one from the total of 12 ligands (Valenzano et al., 2011). However, the comparison was not possible for the rest of materials, due to the uses of different synthetic procedures and conditions, both of which are known to essentially influence the degree of material defects.

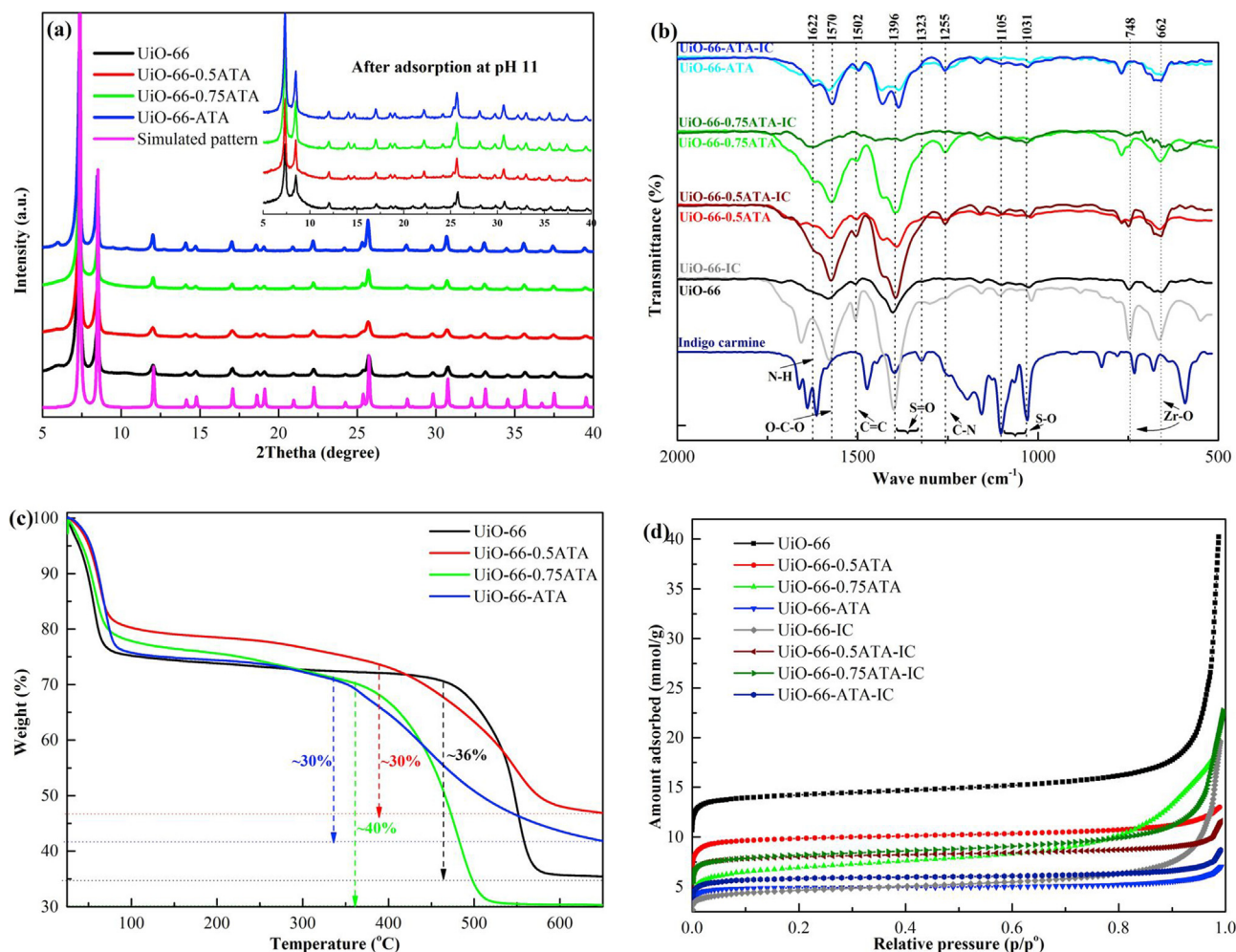


**Figure 1.** (a) PXRD patterns of UiO-66, UiO-66-0.5ATA, UiO-66-0.75ATA and UiO-66-ATA with the inset showing PXRD patterns of the materials after soaking at pH = 11 for 24 h. (b) IR spectra of the pre-adsorbed samples, IC-loaded samples and IC dye (c) TGA plots of the activated UiO-66, UiO-66-0.5ATA, UiO-66-0.75ATA and UiO-66-ATA (d) N<sub>2</sub> gas adsorption isotherms of UiO-66, UiO-66-0.5ATA, UiO-66-0.75ATA and UiO-66-ATA before and after IC adsorption.

Specifically, our used synthesis was carried out without adding any modulator, while others employed it.

By employing elemental analysis, there was a possibility to calculate the number of ATA substitutions in the framework, following the method proposed by Ferreira et al. (2013) The calculated results are tabulated in Table 1. It has been observed from the table that the higher the amount of ATA ligands, the higher the amount of nitrogen mass percentage. The molar proportion of the functionalized linker (%func) of UiO-66-0.5ATA and UiO-66-0.75ATA were determined and found to be 59.20 and 82.89%, respectively. The mismatch between experimental molar proportion and its set value could be hypothesized from the randomly missing ligand vacancy in the materials, at which missing ligands might be BDC rather than ATA. The carbon mass percentage in each material is also shown in Table 1. Again, a slight difference in carbon mass percentage between the experimental and theoretical values of each material could come from the number of missing ligands that cannot be identified.

To assess the porosity of synthesized materials, BET surface area analysis of the adsorbents before and after IC adsorption was conducted. From Figure 1 (d), the nitrogen isotherms of all four materials follow the IUPAC type IV isotherm, thereby confirming the presence of mesopores in their frameworks. However, for UiO-66, the stiff increase of P/P<sub>0</sub> > 0.9 was evident, suggesting macropore presence. Pore size distribution data of UiO-66 shown in Figure S2 confirms the existence of both mesopore and macropore since the distribution of pore with widths of ~32

nm~100 nm was found. The macropore found only in UiO-66 could arise from the defect in the framework generated during the calcination process. In the case of UiO-66, the calcined temperature was 573 K, while those in ML-UiO-66 and UiO-66-ATA were 493 and 473 K, respectively. The higher activation temperature can lead to a higher concentration of defect in UiO-66, which results in larger pore size (Jiao et al., 2017). From Table 2, the parent UiO-66 was found to have a BET surface area of 1281.6 m<sup>2</sup>/g and a total pore volume of 0.4596 cm<sup>3</sup>/g, both of which are highly consistent with values previously reported in the literature for UiO-66 synthesized without using any modulator (Cavka et al., 2008; Wu et al., 2013). In addition, the surface area of materials is observed to have a decreasing trend with an increasing number of ATA ligands connected to the framework, as that of UiO-66-0.5ATA, UiO-66-0.75ATA and UiO-66-ATA were determined to be 877.1, 579.4, and 441.9 m<sup>2</sup>/g, respectively. This is in fact expected since a higher number of ATA means more NH<sub>2</sub> groups, which can protrude into the micropores of the MOFs and thus lead to the subsequent lower surface area (Ezugwu et al., 2019).

Unlike UiO-66, it has been found that obtained surface area of UiO-66-0.5ATA, UiO-66-0.75ATA, and UiO-66-ATA are smaller than those from literature in the order of 1.4, 2.1, and 2.6-folds, respectively. These discrepancies are most likely due to differences in synthetic and activation methods employed in this and other studies (Chavan et al., 2014; Luu et al., 2015). After adsorption, a partial departure of the organic ligand from the framework might occur. This leads to a change in the porosity of the adsorbent. From Table 2, BET surface area of both UiO-66 and

**Table 1.** Molar fraction and mass of organic linkers used in each sample synthesis, the mass percentage of carbon (%C), nitrogen (%N), and hydrogen (%H) obtained from CHON/S elemental analysis and calculated experimental molar proportion of the functionalized linker (%func) (Ferreira et al., 2013; Zhang et al., 2017).

Adsorbents	Mole fraction of BDC and ATA ligand in the synthesis		Experimental mass percentage of C, N and H/(Theoretical mass percentage)*			%func
	X <sub>BDC</sub>	X <sub>ATA</sub>	%C/	%N/	%H/	
UiO-66	1	0	25.827 ± 0.036 (24.17)	-	4.87 ± 0.044 (4.53)	0
UiO-66-0.5ATA	0.5	0.5	25.850 ± 0.046 (23.72)	2.232 ± 0.005 (1.73)	3.854 ± 0.072 (4.07)	59.20
UiO-66-0.75ATA	0.25	0.75	25.886 ± 0.019 (23.58)	3.371 ± 0.022 (2.29)	3.502 ± 0.102 (4.75)	82.89
UiO-66-ATA	0	1	25.888 ± 0.044 (23.29)	3.884 ± 0.046 (3.40)	3.733 ± 0.055 (4.60)	100

\* (Theoretical percentage is calculated based on the perfect UiO-66 and ML-UiO-66 frameworks).

UiO-66-0.5ATA becomes decreased with factors of c.a. 3.3 and 1.23 times lower than those of pre-adsorbed counterparts, respectively. The significant reduction in UiO-66 surface area could have resulted from a combination of partial damages of MOF structure, which were induced during the adsorption process, as well as the pore-filling effect of IC on the macropores between MOF particles. In addition, there could be serious pore blockage by large quantities of IC onto the UiO-66 surface, thereby making the micropores in MOF crystals become no longer accessible for N<sub>2</sub> adsorption. Since the average pore size of the material was found to increase after adsorption, the blocked pores would be micropores, resulting in a decrease of specific surface area. For UiO-66-0.5ATA, similar rationales could be used to explain the material's reduced surface area. In contrast, there were c.a. 1.2-fold increases in surface area of post-adsorbed UiO-66-0.75ATA and UiO-66-ATA. This may originate from the departure of the ATA ligand as ML-UiO-66 and UiO-66-ATA are less stable (Jiao et al., 2017). Once the framework contains less moiety of ATA ligand, the pore entrance becomes more accessible. This might result in the increased surface area obtained in post-adsorbed UiO-66-0.75ATA and UiO-66-ATA, whose pre-adsorbed structures have more ATA ligands than that of UiO-66-0.5ATA. It is also worth mentioning that the porosity of UiO-66 can be tuned via a variation of the number of missing ligand defects. A higher degree of defect can lead to an increase in surface area of UiO-66 and this could be a rational for the observation found in the post-adsorption for UiO-66-0.75ATA and UiO-66-ATA.

### 3.2. Adsorption parameters

Adsorption characteristics such as dye solution pH, adsorbent dosage, dye concentration, and contact duration have a significant impact on an adsorbent's adsorption behavior. Figure 2 (a), (c), and (d) show the effect of the first three adsorption parameters on the adsorption behavior of all studied adsorbents. pH has a direct impact on dye adsorption since changes in pH can drive protonation or deprotonation of adsorbents, as well as ionization of dye molecules. Herein, an effect of solution pH on IC removal by synthesized MOFs was investigated in a range of 2–11 and the results are presented in Figure 2 (a). All synthesized MOFs show a similar trend in their adsorption behavior toward a pH change, where the maximum adsorption capacity was observed at the lowest pH solution of 2.0. With increasing pH, the adsorption capacities drop continuously until reaching their lowest values at a pH of 11. This suggests that electrostatic interaction plays a crucial role during adsorption. Reasonably,

under lower pH, there is a higher degree of H<sup>+</sup> presence in the solution, which promotes the protonation of the adsorbent and thus a positively charged surface as evidenced by zeta potential measurement, as shown in Figure 2 (b). Because of the negatively charged nature of IC, there is a greater electrostatic attraction between the dye molecules and protonated adsorbents, resulting in a higher adsorption capacity. From zeta potential measurement, at a pH of 7, it is evident that adsorbents containing ATA ligand bear a more negatively charged surface than UiO-66. This results in a lower adsorption capacity at every observed pH found in UiO-66-ATA compared to UiO-66. However, when comparing adsorption capacity between UiO-66 and ML-UiO-66, UiO-66-0.75ATA shows the highest overall tested pH, regardless of its more negative charge in nature, while UiO-66-0.5ATA shows higher adsorption capacity at some particular pH. This implies that, apart from electrostatic interaction, other interactions must be involved during the adsorption process. Nevertheless, even at their lowest capacities, all adsorbents still displayed relatively high levels of IC removal in comparison with previous studies (Mittal et al., 2006; Senthil Kumar et al., 2010; Zhang et al., 2016). Their high durability under a harsh pH condition was also ensured, as evidenced from the PRXD result, Figure 1 (a)-inset, which demonstrates that all materials have high crystallinity even after being stirred in a dye solution with a pH of 11 for 24 h. As a result, their use may be guaranteed throughout a wide pH range, improving the simplicity of operation by eliminating the need to alter wastewater pH prior to treatment. Lastly, it is found that IC uptake by all four MOFs follows the order of UiO-66-0.75 > UiO-66-0.5ATA ≈ UiO-66 > UiO-66-ATA at all tested pH values. Furthermore, when compared to previously reported materials, such as activated carbon and carbon nanotube, these four adsorbents show a greater IC adsorption capability (see Table S1). Although the order is not completely aligned with the amount of ATA ligands in the MOFs, it clearly suggests that the mixed component MOF offers an alternative method for enhancing dye adsorption capacity. Nevertheless, there are some certain thresholds that the enhancement can be made.

To investigate the effect of adsorbent dosage on IC removal, the adsorption capacity of IC by four MOFs covering an initial dosage of 10–100 mg was determined using an initial IC concentration of 100 mg/L. As shown in Figure 2 (c), for all four MOFs, the IC removal percentage becomes enhanced with increasing adsorbent dosage until a certain value of dosage, beyond which its further addition begins to have no enhancing effect on the removal. The certain value is called the “threshold dosage”

**Table 2.** Surface characterization of UiO-66, UiO-66-0.5ATA, UiO-66-0.75ATA, and UiO-66-ATA before and after IC adsorption.

Sample	Before adsorption			After IC adsorption		
	BET surface area (m <sup>2</sup> /g)	Pore size (Å)	Pore volume (cm <sup>3</sup> /g)	BET surface area (m <sup>2</sup> /g)	Pore size (Å)	Pore volume (cm <sup>3</sup> /g)
UiO-66	1281.6	14.34	0.4596	389.7	70.20	0.6839
UiO-66-0.5ATA	877.1	20.59	0.4515	711.8	21.80	0.3880
UiO-66-0.75ATA	579.4	46.3	0.6704	708.3	40.66	0.7200
UiO-66-ATA	441.9	22.11	0.2442	512.26	22.78	0.2918

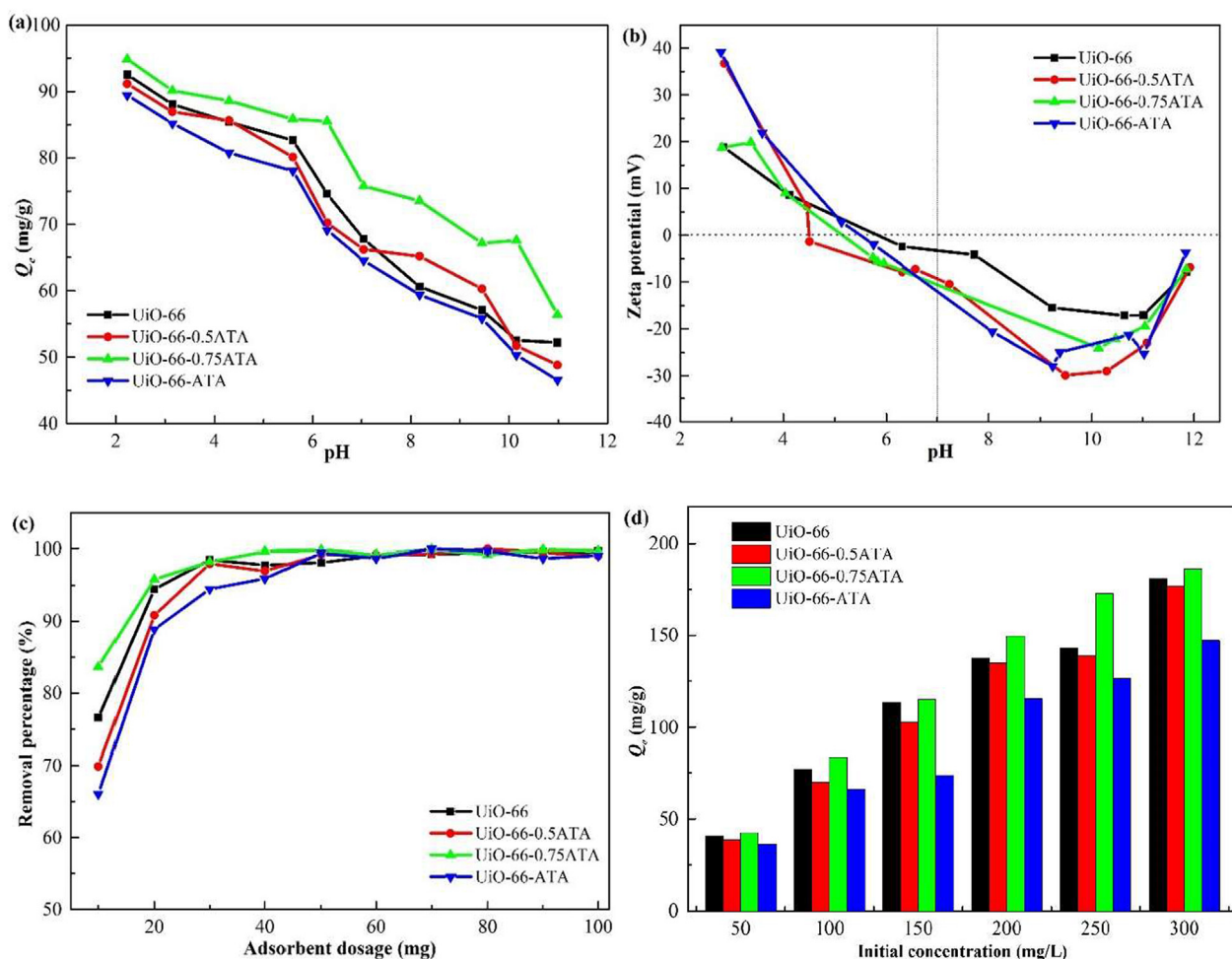


**Figure 2.** (a) The effect of pH on UiO-66, UiO-66-0.5ATA, UiO-66-0.75ATA and UiO-66-ATA adsorption of IC (b) Zeta potential measurement for UiO-66, UiO-66-0.5ATA, UiO-66-0.75ATA and UiO-66-ATA as a function of pH (c) Effect of adsorbent dosage on the percentage of IC removed by UiO-66, UiO-66-0.5ATA, UiO-66-0.75ATA and UiO-66-ATA (d) The influence of IC initial concentration on the adsorption of IC by UiO-66, UiO-66-0.5ATA, UiO-66-0.75ATA and UiO-66-ATA.

and was found to be 30 mg for the two ML-UiO-66 and UiO-66, while that of UiO-66-ATA was determined to be 50 mg. In addition, the greatest degree of enhancement in IC removal by all adsorbents was obtained when their dosage was increased from 10 to 20 mg. After that, only a gentle enhancement in removal was observed, as its percentage was slightly increased. This might be due to agglomeration of solid adsorbents, which reduces the number of adsorbed surface sites (Kumar et al., 2019). In the case of UiO-66-ATA, agglomeration may have less effect, as the materials' frameworks contain amino groups on the surface that may create repulsion forces between particles and result in a more dispersed character.

In this study, the effect of IC initial concentration of 50–300 mg/L on MOFs adsorption capacity was also determined, and its result is presented in Figure 2 (d). From the figure, IC adsorption performance by all MOFs generally increases with increased dye concentration. UiO-66-0.75ATA is the most efficient IC adsorbent among the four MOFs, covering a whole range of IC concentrations. Meanwhile, UiO-66-ATA is the least efficient IC adsorbent. It is worth noting that the IC removal percentage of all four adsorbents decreases with increasing IC concentration due to the limitation of the adsorption sites on the adsorbent surface.

### 3.3. Adsorption kinetics

The effect of contact time on IC removal by the four MOFs for initial IC concentration of 100 mg/L was investigated by varying the contact

time from 0 to 1,440 min, and its result is displayed in Figure 3 (a). From the figure, the adsorption capacity of all MOFs can be enhanced by increasing contact time. Sharp rises in  $Q_e$  during the first contact time of 100 min were usually expected, as during the initial stage, adsorbents still have many free and vacant adsorption sites and thus can rapidly bind with dye molecules present in the solution. As the contact period passes, the majority of the sites are occupied, and the rate of adsorption slows until it achieves a certain value under the equilibrium. For a given IC concentration, a contact time of 480 min appears to be an appropriate duration for all MOFs, beyond which there is a marginal enhancement in  $Q_e$  with time. Nevertheless, a complete equilibrium, where  $Q_e$  becomes virtually constant, is most likely to be attained at the contact time of c.a. 920 minutes.

Adsorption kinetics is of great significance to evaluate the performance of a given adsorbent and understand the underlying mechanisms, both of which control the overall process efficiency and thus are essential for the design of adsorption process facilities. Fundamentally, the adsorption of liquid dyes using solid adsorbent is composed of two sequential steps: (1) the migration of solutes from the bulk solution to the liquid layer adjacent to the adsorbent particle and (2) the diffusion of solutes through the layer until they reach the adsorption surface (film diffusion). Usually, the first step occurs very fast, and thus the second step is the rate-limiting step. However, in a porous adsorbent, an intraparticle diffusion, which particularly refers to the diffusion of solutes into the interior surface of the adsorbent, can also play a role as a rate-controlling step.

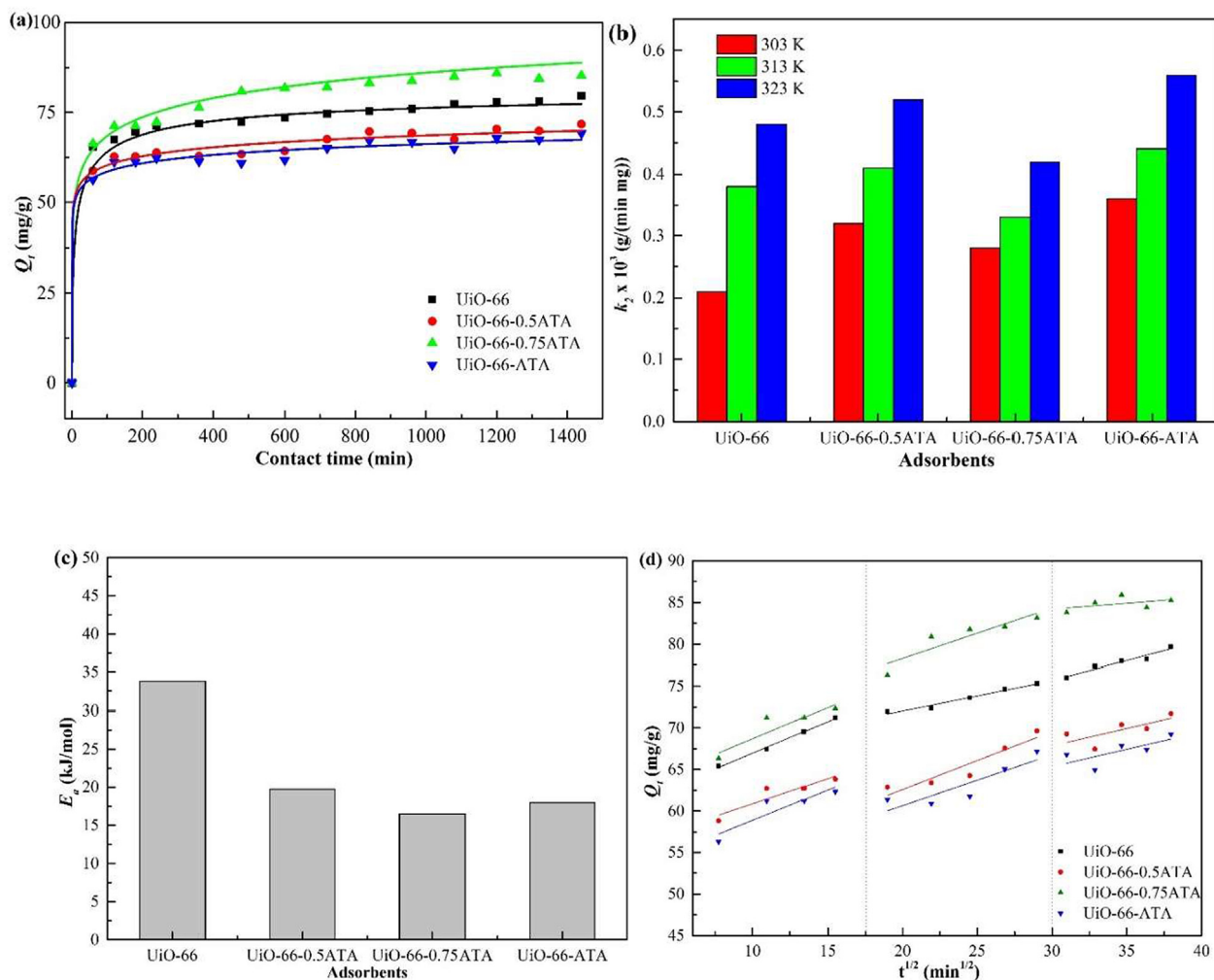


**Figure 3.** (a) The effect of contact duration on IC adsorption by UiO-66, UiO-66-0.5ATA, UiO-66-0.75ATA and UiO-66-ATA at 303 K. (b) Variation of rate constant ( $k_2$ ) with temperature obtained from pseudo-second order model (c) Apparent activation energy ( $E_a$ ) of the IC adsorption. (d) The IPD plots of the IC adsorption by UiO-66, UiO-66-0.5ATA, UiO-66-0.75ATA and UiO-66-ATA at 303 K.

The obtained data from IC adsorption kinetics by all four MOFs under different temperatures, i.e., 303, 313, and 323 K and at initial IC concentration of 100 ppm, were used for the detailed studies of adsorption kinetics using five models, i.e., the pseudo-first-order, pseudo-second-order, Elovich, intraparticle diffusion model (IPD) and Boyd kinetic models. The former three were employed to examine the rate of adsorption of IC from the solution, while the rest of the two models were selected to investigate intraparticle diffusion. The results from fitting our obtained data with models are summarized in Figure S3-7 and Table S2-4 in the Supporting Information.

It has been found that both pseudo-first-order and Elovich models are not suitable in describing IC adsorption kinetics, as poor linear correlation efficiency ( $R^2 < 0.99$ ) was observed for all of the investigated cases, as shown in Table S2, 3, 4. On the other hand, the pseudo-second-order model produced fittings with good quality ( $R^2 > 0.99$ ) as well as a minimal difference between the experimental and theoretical adsorbed masses at equilibrium (less than 1%), suggesting the model's effective simulation capacity and subsequent reliability. As a result, only parameters obtained from the latter model were used for further analysis and discussion. Figure 3 (b) illustrates the effect of temperature and IC concentration on pseudo-second-order rate constant ( $k_2$ ) of each MOF. From the figure, adsorption kinetics of all materials follow an increasing trend with the temperature rise, suggesting the dye adsorption process as an endothermic process. Since UiO-66-ATA was also found to have the

highest rate constant at all three temperatures, this implies a potential role of the amino group in enhancing the rate of adsorption.

Another analysis made of obtained rate constant was the determination of activation energy ( $E_a$ ) by employing the linear form of the Arrhenius equation, which is a plot of  $\ln k_2$  against  $1/T$ , Figure 3 (c). The slope of the plot was then computed to give  $E_a$  for each MOF under an IC concentration of 100 ppm. The figure shows that the values of  $E_a$  of all studied adsorbents are positive which suggests that the adsorption process favors a high temperature, i.e., an endothermic process. An apparent reduction in  $E_a$  values can be observed when ATA ligands were introduced into the UiO-66 framework. It then suggests that amino groups play a vital role in lowering the activation energy of the adsorption process and subsequently enhancing the rate of reaction. Reasonably, amino groups may participate in the attachment of IC molecules during the transition state of adsorption due to their ability to create hydrogen bonding.

Adsorption is a relatively complex process, which usually consists of several consecutive steps. To understand the mechanistic pathway of the IC adsorption in all four MOFs, it becomes necessary first to observe the involved steps of the adsorption and eventually identify the rate-limiting step. Figure 3 (d) shows the fitting of obtained data with the IPD model at 303 K. From this model, if the plot of dye uptake,  $Q_t$ , versus the square root of time,  $t^{1/2}$ , shows linearity, it means that intraparticle diffusion is involved in the adsorption system. Providing the linear plot passes through the origin also implies intraparticle diffusion as the rate-

controlling step. From the figure, it has been found that the adsorption of all four adsorbents exhibits a linear correlation in 3 distinct regions. The first region corresponds to the film diffusion over the first 240 min of adsorption. After this point, the adsorption process is governed by intraparticle diffusion, which consists of surface and pore diffusions, corresponding to regions 2 and 3 in the plot, respectively. Since the rate constants of the first stage ( $k_{1d}$ ) are higher than those of the second ( $k_{2d}$ ) and the third stages ( $k_{3d}$ ) in all four materials, as shown in Table S2, 3, and 4 in the Supporting Information, this finding suggests the potential of intraparticle diffusion being the rate-determining step. However,  $R^2$  values of the fittings show a certain degree of deviation from linearity and the straight lines of each region do not pass through the origin. As a result, these indicate that intraparticle diffusion is not the only rate-limiting step, but other steps may play a role in controlling the adsorption rate, all of which may be co-occurring (Banerjee et al., 2014).

As the conclusion cannot be solely made using the IPD model, further analysis of the data using the Boyd model was carried out. The plots of calculated  $B_t$  versus time of IC adsorption by all four materials at each temperature are provided in Figure S6 in the Supporting Information. The linearity of this plot can be used to distinguish between film diffusion and intraparticle-transport-controlled rate of adsorption. From Figure S6, it can be observed that the plots deviate from linearity under all of the studied conditions and do not pass through the origin, thereby suggesting that film diffusion or external mass transport mainly governs the adsorption process and can be considered as a rate-limiting step. Using the slope of the Boyd plot, values of two model parameters, i.e.,  $B$  and effective diffusion coefficient,  $D_i$  ( $\text{cm}^2/\text{s}$ ), were obtained and listed in Tables S2, 3, and 4. Generally, if  $D_i$  lies in the range  $10^{-11}$  to  $10^{-13}$   $\text{cm}^2/\text{s}$ , intraparticle diffusion is then suggested as the rate-determining step. Since  $D_i$  values of all four materials are in a range of  $1.33\text{--}6.09 \times 10^{-18}$  ( $\text{cm}^2/\text{s}$ ), which is around six orders of magnitude lower, this implies that the intraparticle diffusion was not the only rate-controlling step, but there was also the involvement of film diffusion in controlling adsorption process of IC by synthesized MOFs. Compared to the literature, the  $D_i$  values found in this study are in the same order of magnitude observed from the diffusion rate of organic molecules within other MOFs (Agrawal et al., 2019; Zybalyo et al., 2010).

### 3.4. Adsorption isotherm

To gain insights on the distribution of dye molecules between solid and liquid phases at equilibrium state, the studies of adsorption isotherm

were investigated by fitting our experimental data with four widely employed isotherm models, i.e., Langmuir, Freundlich, Dubunin-Radshbkevish (D-R), and Temkin isotherm models under a given range of temperature. The fittings can be seen in Figure S8-11, and the results obtained from the fittings of each model are summarized in Table 3. In comparison between four models, the Langmuir model is the simplest one, which can only describe the monolayer adsorption in a finite number of homogenous surfaces. The Freundlich model, on the other hand, is better suited to multilayer adsorption on a heterogeneous surface with uneven active sites and varying binding energies. D-R and Temkin models are usually employed to differentiate the type of adsorption mechanism, whether the process is physisorption or chemisorption. By obtaining the isotherm knowledge, the prediction of adsorption capacity and behavior becomes possible and can be used further to elucidate the mechanism of the dye adsorption process.

From Table 3, it has been found that the Langmuir model can effectively describe the process of IC adsorption by three out of four MOFs, i.e., UiO-66-0.5ATA, UiO-66-0.75ATA, and UiO-66-ATA for a whole range of studied temperature with linear correlation coefficient ( $R^2$ ) values of at least 0.99. As a result, these observations suggest the monolayer-typed adsorption for these three materials. In the case of UiO-66, although the model can fit well with data obtained at 303 and 323 K, there was slightly a poorer quality of fitting at 313 K with an  $R^2$  of 0.9724. The maximum values of dye adsorption capacity at equilibrium,  $Q_0$ , for UiO-66, UiO-66-0.5ATA, and UiO-66-ATA, were all observed at 323 K and found to be 454.55, 192.31, and 208.33 mg/g, respectively. In addition, as their values of  $Q_0$  follow an increasing trend with rising temperature, it implies their adsorption processes as endothermic ones. In contrast, for UiO-66-0.75ATA, the maximum  $Q_0$  value of 227.27 mg/g was obtained at 303 K, and its value was found to decrease with increasing temperature, thereby suggesting an exothermic reaction occurred during the IC adsorption process of the material. The “ $b$ ” parameter in the Langmuir model provides information on binding strength and the degree of interaction between the dye and the adsorbent surface. The table shows the common trends of the greater  $b$  value with increasing temperature in all MOFs, except UiO-66, at which the reverse trend can be seen.

In comparison among three MOFs, the order of their  $b$  values follows: UiO-66-0.75 > UiO-66-0.5-ATA > UiO-66-ATA for all investigated temperatures. In other words, the model suggests that the IC adsorption is more favourable on the surface of UiO-66-0.75ATA than the other two adsorbents. The separation factor,  $R_L$ , is another essential parameter of

**Table 3.** Adsorption isotherms parameters of IC adsorption on to UiO-66, UiO-66-0.5ATA, UiO-66-0.75ATA and UiO-66-ATA for Langmuir, Freundlich, Dubunin-Radshbkevish and Temkin models at different temperatures.

Langmuir isotherm	UiO-66			UiO-66-0.5ATA			UiO-66-0.75ATA			UiO-66-ATA		
	303 K	313 K	323 K	303 K	313 K	323 K	303 K	313 K	323 K	303 K	313 K	323 K
$Q_0$ (mg/g)	135.14	303.03	454.55	60.24	175.44	192.31	227.27	192.31	175.44	60.61	196.08	208.33
$b$ (L/g)	0.029	0.032	0.024	0.032	0.059	0.079	0.075	0.077	0.100	0.026	0.040	0.056
$R_L$	0.26	0.24	0.30	0.24	0.14	0.11	0.12	0.11	0.09	0.28	0.20	0.15
$R^2$	0.9930	0.9724	0.9975	0.9930	0.9910	0.9907	0.9966	0.9987	0.9969	0.9993	0.9994	0.9992
Freundlich isotherm												
$K_F$ (mg/g)	20.82	12.33	12.11	10.83	16.04	20.17	25.78	17.68	22.46	11.73	12.65	23.34
$n$	2.99	1.36	1.20	3.32	1.80	1.79	2.10	1.65	1.93	3.49	1.63	2.02
$R^2$	0.9927	0.9941	0.9956	0.9867	0.9736	0.9721	0.965	0.9631	0.9372	0.9819	0.9818	0.9891
Dubunin-Radushkevich isotherm												
$Q_m$ (mg/g)	101.49	157.43	175.56	51.99	131.76	141.32	176.09	143.31	134.83	44.08	133.49	143.02
$E$ (kJ/mol)	0.10	0.18	0.21	0.06	0.17	0.24	0.16	0.25	0.30	0.46	0.49	0.21
$R^2$	0.9000	0.9394	0.9525	0.9059	0.9159	0.8887	0.8852	0.9159	0.8688	0.9160	0.9380	0.9255
Temkin isotherm												
$B$	28.01	66.22	79.54	11.77	34.60	37.43	46.69	34.48	34.87	13.56	46.61	48.08
$b$ (J/mol)	89.93	39.30	33.76	213.96	75.20	71.75	53.96	67.63	77.01	185.72	55.83	55.86
$A$ (L/mg)	0.33	0.3	0.32	0.45	0.79	1.06	0.68	0.97	1.27	0.24	0.33	0.49
$R^2$	0.9964	0.9767	0.9897	0.9804	0.9756	0.9743	0.9974	0.9791	0.9961	0.9997	0.9990	0.9988

Langmuir isotherm and can predict the affinity between adsorbate and adsorbent. As all  $R_L$  values determined from all four materials were found to lie between 0 and 1 (ranging from 0.09 to 0.30), the results then suggest favourable nature of the IC adsorption process by all MOFs under a whole range of given temperature. Herein, a decreasing trend of  $R_L$  with rising temperature was mutually observed in ML-UiO-66 and UiO-66-ATA, indicating the IC adsorption process to become more favourable at higher temperatures. Again, the uncommon finding in UiO-66 could be rationalized as mentioned above.

As the second choice of isotherm, the Freundlich model was found to fit well with experimental data obtained from UiO-66 with all  $R^2$  values of above 0.99, but give poorer fitting result for the rest of the three materials, as evidenced from their  $R^2$  values of below 0.99, as shown in Table 3. Therefore, this suggests the Freundlich model as a more suitable one over the Langmuir for describing the IC adsorbing behavior of UiO-66 as well as implies the heterogeneity of material surface with different binding energies on its surface. Besides, as the model cannot simulate the adsorption process of ML-UiO-66 and UiO-66-ATA effectively, our discussion will be made related to solely UiO-66. Regarding the Freundlich model, there are two constants, i.e.,  $n$  and  $K_F$ , indicating adsorption intensity and capacity, respectively. Specifically, the value of  $n$  determines the degree of nonlinearity between the concentration of dye solution and its adsorption quantity in two different ways: 1) if  $n < 1$ , the adsorption process is chemisorption, and 2) if  $n > 1$ , the adsorption process is physisorption (Senthil Kumar et al., 2010). As shown in the table, since  $n$  values obtained from all studied conditions are greater than 1, it implies the IC adsorption process by UiO-66 as physisorption rather than chemisorption process. In addition, the value of  $1/n$  can be used to infer a favourable adsorption under all of the experimental conditions, as its value is in between 0 and 1. Both  $K_F$  and  $1/n$  display an increasing profile with increasing temperature, indicating a more favourable adsorption process at a higher temperature. These findings in UiO-66 are essentially similar to ones previously observed in ML-UiO-66 and UiO-66-ATA using the Langmuir model.

Among four models, the worst fitting was observed in the D-R model, with none of the  $R^2$  values reaching 0.99, implying the model as an invalid option for further investigation and discussion. For the Temkin model, considering all  $R^2$  determined can provide relatively good fitting with a comparable degree with that obtained from the Freundlich model. Nevertheless, the results show UiO-66-ATA as the most suitable material, whose IC adsorption process can be described by the model, as its  $R^2$  values of the fittings are greater than 0.99 for all studied temperatures. Since Temkin isotherm considers the effect of the heat of adsorption through its constant “ $b$ ”, its suitable fittings in all four MOFs suggest the IC adsorption process by materials to be highly dependent on this type of heat. Under our experimental specification, as all of the  $b$  values determined are less than 1 kcal/mol (4,184 J/mol), it then confirms the physisorption nature in UiO-66 adsorption, as previously revealed by the Freundlich model, as well as suggests the same reaction nature for the process carried out by the rest of three materials. Lastly, the model also infers all the adsorption processes as exothermic reactions, as all  $A$  values are positive.

**3.5 Adsorption thermodynamics.**  
To determine the spontaneity of adsorption processes from the view of the energetic driving force, the study of IC adsorption thermodynamics was performed by plotting  $\ln K_d$  versus  $1/T$ , see Figure S12 and the enthalpy ( $\Delta H$ ), entropy ( $\Delta S$ ), and Gibbs free energy ( $\Delta G$ ) of all four MOFs under 303, 313, and 323 K were calculated. The results are listed in Table 4.

It has been revealed from the table that all IC adsorption processes by synthesized materials are endothermically driven ( $\Delta H > 0$ ), the finding which is in line with the studies as mentioned earlier of adsorption kinetics and isotherm. This means that the IC adsorption process favors higher temperature, similar to what have been reported in other types of dyes adsorption by UiO-66 analogues (Molavi et al., 2018). Reasonably, the increase in temperature not only enhances rate of adsorption reaction, but also provides more energy to dye molecules, making them

**Table 4.** Enthalpy, entropy, and Gibbs free energy for the adsorption of IC onto the UiO-66, UiO-66-0.5ATA, UiO-66-0.75ATA and UiO-66-ATA.

Adsorbent	$\Delta H^\circ$ (kJ/mol)	$\Delta S^\circ$ (J/mol K)	$\Delta G^\circ$ (kJ/mol)			$R^2$
			303 K	313 K	323 K	
UiO-66	36.38	132.72	-3.73	-5.40	-6.37	0.9708
UiO-66-0.5ATA	79.39	270.65	-2.17	-6.30	-7.52	0.9009
UiO-66-0.75ATA	9.20	52.40	-6.74	-7.06	-7.79	0.8646
UiO-66-ATA	81.16	273.67	-1.25	-5.61	-6.65	0.8802

become more energetic and can easily pass through the micropore of the adsorbent (Al-Ghouthi and Al-Absi, 2020). Based on the value of  $\Delta H$ , the mechanism of the adsorption process can also be inferred: 1) when  $\Delta H$  is in the range of 8–65 kJ/mol, the adsorption process is physisorption and 2) when  $\Delta H$  is in the range of 84–420 kJ/mol, the adsorption process is chemisorption (Hu et al., 2014). As a result, by following this criteria, the adsorption processes in both UiO-66 and UiO-66-0.75ATA are classified as physisorption. In the case of both UiO-66-0.5ATA and UiO-66-ATA, as their values of  $\Delta H$  do not fall into the given criteria but are greater than the upper range of the physisorption, it then suggests their processes to be a physicochemical reaction, potentially having chemisorption as a dominant mechanism (Li et al., 2011). Having considered  $\Delta S$ , their positive values, which means an increase in disorder, were resulted from the total entropy change of the two processes during liquid phase adsorption, including dye molecule adsorption and water desorption. The first leads to a decrease in freedom, while the latter causes an opposite effect. As water molecules are smaller than IC molecules, much more desorbed water is generated. The higher amount of generated water then leads to a greater contribution of water desorption to the entropy change of a system (Li et al., 2015). The positivity of both  $\Delta H$  and  $\Delta S$  suggests the adsorption as an endothermic process driven by a favourable change in system entropy. These findings are found to be in good agreement with previous adsorption studies (Kishani et al., 2021). The spontaneity of all studied processes was additionally confirmed by negative values of determined Gibbs free energy. Furthermore, the fact that  $\Delta G$  becomes more negative with increasing temperature shows that the degree of spontaneity in all reactions is dependent on temperature and can be enhanced at a higher temperature. The value of  $\Delta G^\circ$  can differentiate between physisorption ( $-20 - 0$  kJ mol<sup>-1</sup>) and the chemisorption process ( $-400 - -80$  kJ mol<sup>-1</sup>). All the determined  $\Delta G^\circ$  in Table 4 suggest physisorption mechanisms for IC adsorption on all candidate materials.

### 3.5. Adsorption mechanism

Considering the results obtained from all the studies mentioned earlier gives us the possible mechanism that dictates the adsorption behavior of IC onto synthesized adsorbents. The core factor regulating the adsorption process is the surface interaction between adsorbent and adsorbate, which can be physical or chemical forces. In this study, the adsorption processes of IC by all four materials were found to be physisorption. In addition, IR spectra show no shift/extra in characteristic vibrational peaks but rather the characteristic peaks of both adsorbents and IC dye together (Figure 1 (b)). This means that IC dye molecules were adsorbed onto the adsorbent surface without forming chemical bonding. Since the attachment of IC molecules on the UiO-66 surface has been discovered to be multilayer, it suggests the uneven energy of the adsorption sites, which could be caused by partial ligand missing as observed in UiO-66. For ML-UiO-66 and UiO-66-ATA, adsorption of dye molecules occurred in a monolayer pattern, implying homogeneity of their surfaces. The finding of the latter three opposes that of UiO-66, even though all the materials contain certain degrees of missing ligand. As such, it may be possible that the presence of amino groups in these three MOFs makes their surfaces with defect sites become more steric and then more unreachable from approaching dye molecules. Once attached to the

surface, it can be inferred that attached IC molecules remain on the surface, as molecular dye size is larger than an aperture of all adsorbents, resulting in disregard of pore/size-selective adsorption (Doménech et al., 2007). As there are several underlying forces, e.g., electrostatic force, van der Waal interaction, and  $\pi$ - $\pi$  stacking and hydrogen bonding in physisorption, it is crucial to identify the one that dominates the process. Since the adsorption of all four materials is pH-dependent, this suggests electrostatic or acid-base interaction as a potential governing force. Due to the anionic nature of IC dye, an adsorbent surface with a less negative nature can effectively facilitate electrostatic interaction and the subsequent adsorption. As evidenced in Figure 2 (b), the zeta potential of ML-UiO-66 and UiO-66-ATA are close in magnitude and more negative than that of UiO-66, thereby suggesting the potential effect of amino groups in the induction of more negatively charged surface and

subsequently greater repulsion force. Acid-base interaction can occur in the adsorption process by MOFs, as the missing ligand defects of the materials lead to the generation of Lewis acid sites. These generated sites are later induced by water in dye solution to become both Brønsted acid/base sites. IC dye, a Brønsted base, then interacts with these sites (Caratelli et al., 2017). The presence of amino groups was also reported to strengthen the bonding of water at the Brønsted acid sites, which could weaken acid-base interaction in both ML-UiO-66 and UiO-66-ATA and give rise to their lower adsorption capacity, in comparison with that of UiO-66. As shown in Figure 2 (a), the highest adsorption capacities of all four materials were obtained under the most acidic condition. In principle, this would not have been observed if acid-base interaction was the dominant force. Reasonably, under highly acidic conditions, IC molecules become completely protonated and thus can no longer interact with

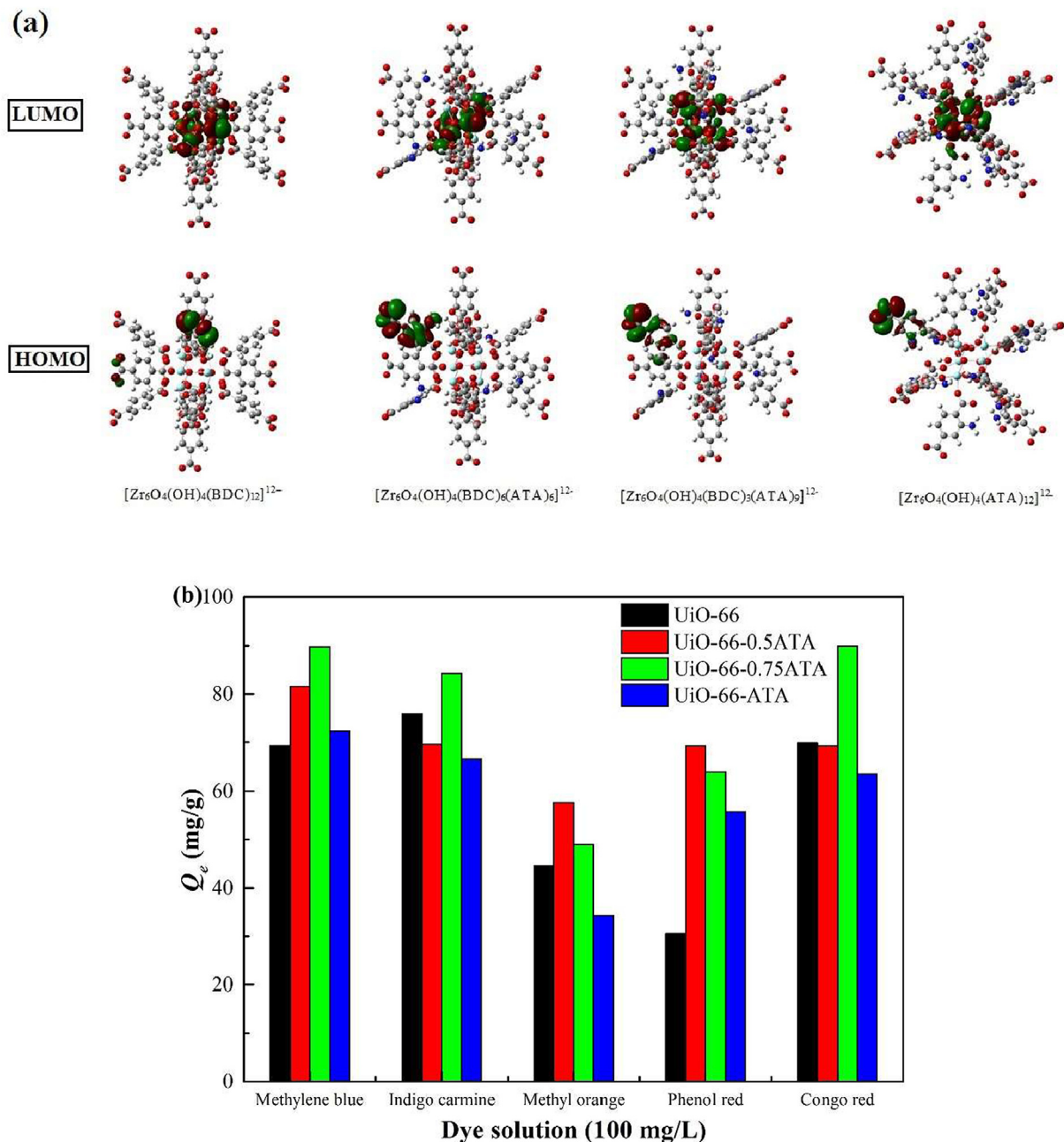


**Figure 4.** (a) The selected excited state molecular orbitals (LUMO) of  $[\text{Zr}_6\text{O}_4(\text{OH})_4(\text{OOC}-\text{C}_6\text{H}_4-\text{COO})_{12}]^{12-}$ ,  $[\text{Zr}_6\text{O}_4(\text{OH})_4(\text{OOC}-\text{C}_6\text{H}_4-\text{COO})_6(\text{OOC}-\text{C}_6\text{H}_6\text{N}-\text{COO})_6]^{12-}$ ,  $[\text{Zr}_6\text{O}_4(\text{OH})_4(\text{OOC}-\text{C}_6\text{H}_4-\text{COO})_3(\text{OOC}-\text{C}_6\text{H}_6\text{N}-\text{COO})_9]^{12-}$  and  $[\text{Zr}_6\text{O}_4(\text{OH})_4(\text{OOC}-\text{C}_6\text{H}_6\text{N}-\text{COO})_{12}]^{12-}$  calculating at PBE1PBE/LanL2DZ level of accuracy (b) Adsorption capacity of UiO-66, UiO-66-0.5ATA, UiO-66-0.75ATA and UiO-66-ATA at different types of dyes solution (dye concentration = 100 ppm, pH = 6.5, contact time = 24 h, adsorbent dosage = 10.0000 mg in 10.00 mL dye solution).

absorbents. As a result, this indicates a small influence of acid-base interactions in respective adsorption performance.

The other possible interactions, including  $\pi$ - $\pi$  stacking and hydrogen bonding, may also occur during the adsorption process. For  $\pi$ - $\pi$  stacking, the interaction can be formed in all four MOFs since all materials have benzene rings, interacting with quasiplanar IC molecules. In contrast, hydrogen bonding can only exist in the adsorption of MOFs containing amino groups, i.e., ML-UiO-66 and UiO-66-ATA. Nevertheless, hydrogen bonding cannot be regarded as the main force since the highest IC removal capacity was observed from UiO-66-0.75ATA, the MOFs bearing some amino groups, as evidenced in Figure 2 (a). Although the presence of amino group does not give many benefits to adsorption capacity, it possibly assists the attachment of dye molecules on the surface of ML-UiO-66 and UiO-66-ATA, then resulting in their lower activation energy and faster adsorption rate, as shown in Figure 3 (b) and (c).

To further investigate how the introduction of ATA ligand affects the framework at the molecular level, and thus may give a clue on how it affects the adsorption behavior, all possible structures of SBU-ligands cluster were optimized at PM6 level, see Figure S13. The study of orbital contributions in the adsorbents before and after adsorption (ground state and excited state) was carried out using TD-DFT. In addition, HOMO and LUMO of one perfect SBU-ligands cluster of all four materials were also investigated, see Figure S14. Previously, the method was employed with a successful investigation of UiO-66 and its analogue under light absorption (Hendrickx et al., 2015). From Figure 4 (a), it is evident that HOMO in all four adsorbents were localized on the organic linker. Upon excitation, the orbital contribution shifted from its initial position to the inorganic cluster, specifically at Zr atoms. This suggests the role of the organic linker and inorganic cluster as electron-donating and accepting units. However, the pattern of LUMO localization on the inorganic cluster was observed to be different from one adsorbent to another. In UiO-66, LUMO localized almost evenly on all six Zr atoms, while in the case of UiO-66-ATA, the LUMO distribution per Zr atom was unequal. For ML-UiO-66, as the substitution of ATA ligand into the framework was random, various patterns were observed. Specifically, in UiO-66-0.5ATA, two patterns were observed; (1) evenly localized LUMO on all six Zr atoms similar to UiO-66 and (2) evenly localized LUMO on only four Zr atoms. Interestingly, in the case of UiO-66-0.75ATA, only one pattern of orbital contribution existed where LUMO localized heavily on only four Zr atoms. This means the substitution of the functionalized ligand into the framework greatly influences the distribution of electron densities in the framework. The results obtained from theoretical calculation show the disappearance of the orbital contribution of organic ligand, producing a significant shift of the orbital contributions toward the inorganic metal cluster theoretically. This indicates a vital role of organic ligand in determining the charge character of the cluster. Hypothetically, without an amino group, the electron density at inorganic clusters of UiO-66 possibly distributes equally, generating a lower degree of electrostatic repulsion between adsorbent surface and anionic dyes, eventually higher capacity of removal. Meanwhile, in UiO-66-ATA, the opposite phenomenon occurred and thus resulted in its lower adsorbing capacity.

To support the proposed mechanism, adsorption of all four adsorbents toward the different character of charged dyes were studied, and the results are shown in Figure 4 (b) and Table S5. UiO-66 shows higher adsorption capacity compared to UiO-66-ATA when tested with anionic dyes such as IC and methyl orange (MO). On the contrary, a greater adsorption capacity is achieved by UiO-66-ATA in the case of a cationic dye such as methylene blue (MB). Interestingly, in every dye system, ML-UiO-66 has a better adsorption capacity than its parent MOFs. This shows that numerous interactions work together to control the adsorption process. A mixed ligand approach can thus be one of the alternatives to engineer this interaction harmony. Noticeably, by employing a mixed ligand approach, the adsorption capacity can be enhanced albeit with less impact than the mixed metal approach (Yang et al., 2018). This could be hypothesized that the former approach only indirectly manipulates the

cluster charge density, whereas the direct influence can be caused by the latter.

#### 4. Conclusion

UiO-66 is an excellent compound choice for dye adsorption because of its unique properties. This study proves an introduction of ATA ligands into the material framework as a promising way to enhance and regulate its adsorption process. The introduced ATA ligands show to have direct and simultaneous influences on several intrinsic parameters of the material at the molecular level, which lead to changes in its macromolecular characters. Despite the interest and potential of the mixed ligand approach, a common trend in its effect does not exist, making the mean still uncontrollable. As a result, it indicates a crucial necessity for future works to be carried out to optimize the system. Moreover, as all adsorbents exhibit a certain degree of defect which also participates in the adsorption process, future work on how defects affect dye adsorption behavior should be carried out experimentally and theoretically.

#### Declarations

##### Author contribution statement

Chompoonoot Nanthamathee: Conceived and designed the experiments; Performed the experiments; Analyzed and interpreted the data; Contributed reagents, materials, analysis tools or data; Wrote the paper.

Chantamalinee Chantarangkul, Chanida Jakkrawhad, Apirak Payaka: Performed the experiments; Wrote the paper.

Pongsathorn Dechatiwongse: Analyzed and interpreted the data; Contributed reagents, materials, analysis tools or data; Wrote the paper.

##### Funding statement

This work was supported by Walailak University (WU-63211) and Thailand Science Research and Innovation Fund (FRB650082/0227).

##### Data availability statement

Data included in article/supplementary material/referenced in article.

##### Declaration of interests statement

The authors declare no conflict of interest.

##### Additional information

Supplementary content related to this article has been published online at <https://doi.org/10.1016/j.heliyon.2022.e08961>.

#### Acknowledgements

The authors would also like to thank University of Malaya for computational facilities and calculation programs.

#### References

- Agrawal, M., Boufelfel, S.E., Sava Gallis, D.F., Greathouse, J.A., Sholl, D.S., 2019. Determining diffusion coefficients of chemical warfare agents in metal-organic frameworks. *J. Phys. Chem. Lett.* 10, 7823-7830.
- Ahmadijokani, F., Mohammadkhani, R., Ahmadipouya, S., Shokrgozar, A., Rezakazemi, M., Molavi, H., Aminabhavi, T.M., Arjmand, M., 2020. Superior chemical stability of UiO-66 metal-organic frameworks (MOFs) for selective dye adsorption. *Chem. Eng. J.* 399, 125346.
- Al-Ghouti, M.A., Al-Absi, R.S., 2020. Mechanistic understanding of the adsorption and thermodynamic aspects of cationic methylene blue dye onto cellulosic olive stones biomass from wastewater. *Sci. Rep.* 10, 15928.

- Banerjee, S., Sharma, G.C., Chattopadhyaya, M.C., Sharma, Y.C., 2014. Kinetic and equilibrium modeling for the adsorptive removal of methylene blue from aqueous solutions of activated fly ash (AFSH). *J. Environ. Chem. Eng.* 2, 1870–1880.
- Caratelli, C., Hajek, J., Cirujano, F.G., Waroquier, M., Labrés i Xamena, F.X., Van Speybroeck, V., 2017. Nature of active sites on UiO-66 and beneficial influence of water in the catalysis of Fischer esterification. *J. Catal.* 352, 401–414.
- Cavka, J.H., Jakobsen, S., Olsbye, U., Guilloleau, N., Lamberti, C., Bordiga, S., Lillerud, K.P., 2008. A new zirconium inorganic building brick forming metal organic frameworks with exceptional stability. *J. Am. Chem. Soc.* 130, 13850–13851.
- Chavan, S.M., Shearer, G.C., Svelle, S., Olsbye, U., Bonino, F., Ethiraj, J., Lillerud, K.P., Bordiga, S., 2014. Synthesis and characterization of amine-functionalized mixed-ligand metal-organic frameworks of UiO-66 topology. *Inorg. Chem.* 53, 9509–9515.
- Chen, C., Zhang, M., Guan, Q., Li, W., 2012. Kinetic and thermodynamic studies on the adsorption of xylenol orange onto MIL-101(Cr). *Chem. Eng. J.* 183, 60–67.
- Desore, A., Narula, S.A., 2018. An overview on corporate response towards sustainability issues in textile industry. *Environ. Dev. Sustain.* 20, 1439–1459.
- Doménech, A., Doménech-Carbó, M.T., Vázquez de Agredos Pascual, M.L., 2007. Indigo/dehydroindigo/palygorskite complex in maya blue: an electrochemical approach. *J. Phys. Chem. C* 111, 4585–4595.
- Ezugwu, C.I., Zhang, S., Li, S., Shi, S., Li, C., Verpoort, F., Yu, J., Liu, S., 2019. Efficient transformative HCHO capture by defective NH<sub>2</sub>-UiO-66(Zr) at room temperature. *Environ. Sci. Nano* 6, 2931–2936.
- Ferreira, R.B., Scheetz, P.M., Formiga, A.L.B., 2013. Synthesis of amine-tagged metal-organic frameworks isostructural to MIL-101(Cr). *RSC Adv.* 3, 10181–10184.
- Freundlich, H.M.F., 1906. Over the adsorption in solution. *Phys. Chem.* 57, 385–471.
- Frisch, M.J., G.W.T., Schlegel, H.B., Scuseria, G.E., Robb, M.A., Cheeseman, J.R., Scalmani, G., Barone, V., Petersson, G.A., Nakatsuji, H., Li, X., Caricato, M., Marenich, A., Bloino, J., Janesko, B.G., Gomperts, R., Mennucci, B., Hratchian, H.P., Ortiz, J.V., Izmaylov, A.F., Sonnenberg, J.L., Williams-Young, D., Ding, F., Lipparini, F., Egidi, F., Goings, J., Peng, B., Petrone, A., Henderson, T., Ranasinghe, D., Zakrzewski, V.G., Gao, J., Rega, N., Zheng, G., Liang, W., Hada, M., Ehara, M., Toyota, K., Fukuda, R., Hasegawa, J., Ishida, M., Nakajima, T., Honda, Y., Kitao, O., Nakai, H., Vreven, T., Throssell, K., Montgomery Jr., J.A., Peralta, J.E., Ogliaro, F., Bearpark, M., Heyd, J.J., Brothers, E., Kudin, K.N., Staroverov, V.N., Keith, T., Kobayashi, R., Normand, J., Raghavachari, K., Rendell, A., Burant, J.C., Iyengar, S.S., Tomasi, J., Cossi, M., Millam, J.M., Klene, M., Adamo, C., Cammi, R., Ochterski, J.W., Martin, R.L., Morokuma, K., Farkas, O., Foresman, J.B., Fox, D.J., 2016. Gaussian, Inc., Wallingford CT. Gaussian, Inc. Gaussian 09.
- Han, Y., Liu, M., Li, K., Sun, Q., Zhang, W., Song, C., Zhang, G., Conrad Zhang, Z., Guo, X., 2017. In situ synthesis of titanium doped hybrid metal-organic framework UiO-66 with enhanced adsorption capacity for organic dyes. *Inorg. Chem. Front.* 4, 1870–1880.
- Hasan, Z., Khan, N.A., Jung, S.H., 2016. Adsorptive removal of diclofenac sodium from water with Zr-based metal-organic frameworks. *Chem. Eng. J.* 284, 1406–1413.
- Hendrickx, K., Vanpoucke, D.E.P., Leus, K., Lejaeghere, K., Van Yperen-De Deyne, A., Van Speybroeck, V., Van Der Voort, P., Hemelsoet, K., 2015. Understanding intrinsic light absorption properties of UiO-66 frameworks: a combined theoretical and experimental study. *Inorg. Chem.* 54, 10701–10710.
- Hu, J., Yu, H., Dai, W., Yan, X., Hu, X., Huang, H., 2014. Enhanced adsorptive removal of hazardous anionic dye “Congo red” by a Ni/Cu mixed-component metal-organic porous material. *RSC Adv.* 4, 35124–35130.
- Huo, S.-H., Yan, X.-P., 2012. Metal-organic framework MIL-100(Fe) for the adsorption of malachite green from aqueous solution. *J. Mater. Chem.* 22, 7449–7455.
- Jiao, Y., Liu, Y., Zhu, G., Hungerford, J.T., Bhattacharyya, S., Lively, R.P., Sholl, D.S., Walton, K.S., 2017. Heat-treatment of defective UiO-66 from modulated synthesis: adsorption and stability studies. *J. Phys. Chem. C* 121, 23471–23479.
- Kishani, S., Bensefelt, T., Wågberg, L., Wohlert, J., 2021. Entropy drives the adsorption of xyloglucan to cellulose surfaces – a molecular dynamics study. *J. Colloid Interface Sci.* 588, 485–493.
- Kumar, K.V., Gadipelli, S., Wood, B., Ramisetty, K.A., Stewart, A.A., Howard, C.A., Brett, D.J.L., Rodriguez-Reinoso, F., 2019. Characterization of the adsorption site energies and heterogeneous surfaces of porous materials. *J. Mater. Chem.* 7, 10104–10137.
- Langmuir, I., 1916. The constitution and fundamental properties of solids and liquids. Part I. Solid. *J. Am. Chem. Soc.* 38, 2221–2295.
- Li, X., Zhou, X., Mu, J., Lu, L., Han, D., Lu, C., Wang, M., 2011. Thermodynamics and kinetics of p-aminophenol adsorption on poly(aryl ether ketone) containing pendant carboxyl groups. *J. Chem. Eng. Data* 56, 4274–4277.
- Li, C., Xiong, Z., Zhang, J., Wu, C., 2015. The strengthening role of the amino group in metal-organic framework MIL-53 (Al) for methylene blue and malachite green dye adsorption. *J. Chem. Eng. Data* 60, 3414–3422.
- Luu, C.L., Nguyen, T.T.V., Nguyen, T., Hoang, T.C., 2015. Synthesis, characterization and adsorption ability of UiO-66-NH<sub>2</sub>. *Adv. Nat. Sci. Nanosci. Nanotechnol.* 6, 025004.
- Masoomi, M.Y., Morsali, A., Dhakshinamoorthy, A., Garcia, H., 2019. Mixed-metal MOFs: unique opportunities in metal-organic framework (MOF) functionality and design. *Angew. Chem. Int. Ed.* 58, 15188–15205.
- Mittal, A., Mittal, J., Kurup, L., 2006. Batch and bulk removal of hazardous dye, indigo carmine from wastewater through adsorption. *J. Hazard Mater.* 137, 591–602.
- Mohammadi, A.A., Alinejad, A., Kamarehie, B., Javan, S., Ghaderpoory, A., Ahmadvour, M., Ghaderpoori, M., 2017. Metal-organic framework UiO-66 for adsorption of methylene blue dye from aqueous solutions. *Int. J. Environ. Sci. Technol.* 14, 1959–1968.
- Molavi, H., Hakimian, A., Shojaei, A., Raeiszadeh, M., 2018. Selective dye adsorption by highly water stable metal-organic framework: long term stability analysis in aqueous media. *Appl. Surf. Sci.* 445, 424–436.
- Nanthamathée, C., 2019. Effect of Co(II) dopant on the removal of Methylene Blue by a dense copper terephthalate. *J. Environ. Sci.* 81, 68–79.
- Qiu, J., Feng, Y., Zhang, X., Jia, M., Yao, J., 2017. Acid-promoted synthesis of UiO-66 for highly selective adsorption of anionic dyes: adsorption performance and mechanisms. *J. Colloid Interface Sci.* 499, 151–158.
- Rego, R.M., Sriram, G., Ajeya, K.V., Jung, H.-Y., Kurkuri, M.D., Kigga, M., 2021. Cerium based UiO-66 MOF as a multipollutant adsorbent for universal water purification. *J. Hazard Mater.* 416, 125941.
- Salama, R.S., El-Sayed, E.-S.M., El-Bahy, S.M., Awad, F.S., 2021. Silver nanoparticles supported on UiO-66 (Zr): as an efficient and recyclable heterogeneous catalyst and efficient adsorbent for removal of indigo carmine. *Colloids Surf. A Physicochem. Eng. Asp.* 626, 127089.
- Senthil Kumar, P., Ramalingam, S., Senthamarai, C., Niranjana, M., Vijayalakshmi, P., Sivanesan, S., 2010. Adsorption of dye from aqueous solution by cashew nut shell: studies on equilibrium isotherm, kinetics and thermodynamics of interactions. *Desalination* 261, 52–60.
- Singh, P.K., Banerjee, S., Srivastava, A.L., Sharma, Y.C., 2015. Kinetic and equilibrium modeling for removal of nitrate from aqueous solutions and drinking water by a potential adsorbent, hydrous bismuth oxide. *RSC Adv.* 5, 35365–35376.
- Thiry, M.C., 2011. Staying Alive: Making Textiles Sustainable.
- Valenzano, L., Civalieri, B., Chavan, S., Bordiga, S., Nilsen, M.H., Jakobsen, S., Lillerud, K.P., Lamberti, C., 2011. Disclosing the complex structure of UiO-66 metal organic framework: a synergic combination of experiment and theory. *Chem. Mater.* 23, 1700–1718.
- Wu, H., Chua, Y.S., Krungleviciute, V., Tyagi, M., Chen, P., Yildirim, T., Zhou, W., 2013. Unusual and highly tunable missing-linker defects in zirconium metal-organic framework UiO-66 and their important effects on gas adsorption. *J. Am. Chem. Soc.* 135, 10525–10532.
- Xu, Y., Jin, J., Li, X., Han, Y., Meng, H., Wang, T., Zhang, X., 2015. Fabrication of hybrid magnetic HKUST-1 and its highly efficient adsorption performance for Congo red dye. *RSC Adv.* 5, 19199–19202.
- Yang, J.-M., 2017. A facile approach to fabricate an immobilized-phosphate zirconium-based metal-organic framework composite (UiO-66-P) and its activity in the adsorption and separation of organic dyes. *J. Colloid Interface Sci.* 505, 178–185.
- Yang, J.-M., Ying, R.-J., Han, C.-X., Hu, Q.-T., Xu, H.-M., Li, J.-H., Wang, Q., Zhang, W., 2018. Adsorptive removal of organic dyes from aqueous solution by a Zr-based metal-organic framework: effects of Ce(III) doping. *Dalton Trans.* 47, 3913–3920.
- Zhang, J., Zhou, Q., Ou, L., 2016. Removal of indigo carmine from aqueous solution by microwave-treated activated carbon from peanut shell. *Desalination Water Treat.* 57, 718–727.
- Zhang, N., Yuan, L.-Y., Guo, W.-L., Luo, S.-Z., Chai, Z.-F., Shi, W.-Q., 2017. Extending the use of highly porous and functionalized MOFs to Th(IV) capture. *ACS Appl. Mater. Interfaces* 9, 25216–25224.
- Zybaylo, O., Shekhah, O., Wang, H., Tafipolsky, M., Schmid, R., Johannsmann, D., Wöll, C., 2010. A novel method to measure diffusion coefficients in porous metal-organic frameworks. *Phys. Chem. Chem. Phys.* 12, 8093–8098.